GEOLOGICA CARPATHICA, JUNE 2013, 64, 3, 231–236 doi: 10.2478/geoca-2013-0017

Native selenium as a byproduct of microbial oxidation of distorted pyrite crystals: the first occurrence in the Carpathians

ELIGIUSZ SZEŁĘG, JANUSZ JANECZEK✉ and PAWEŁ METELSKI

University of Silesia, Faculty of Earth Sciences, Będzińska ul. 60, 41-200 Sosnowiec, Poland;
eligiusz.szeleg@us.edu.pl; ✉janusz.janeczek@us.edu.pl; pawel.metelski@o2.pl

(Manuscript received August 16, 2012; accepted in revised form March 14, 2013)

Abstract: Acicular crystals of native selenium up to 30 μm long occur together with barite on the surface of goethite partial pseudomorphs after millimeter-sized pseudotetragonal-prismatic pyrite crystals in calcite veins that cross-cut Senonian sandstones of the Silesian Nappe in the western Polish Outer Carpathians. Native selenium originated from selenium apparently released during bacteria-induced oxidation of pyrite at neutral or near-neutral pH conditions. Oxidizing bacteria preferentially colonized {100} faces of pyrite relative {111} faces.

Key words: Outer Carpathians, Poland, bacterial oxidation, goethite, pyrite, native selenium.

Introduction

Inspection of calcite veins that cross-cut thick-bedded sandstone in the Silesian Beskid Mountains of the western Polish Outer Carpathians has revealed the abundance of pyrite displaying various crystal habits including distorted (elongated) pseudo-tetragonal prismatic forms and malformed crystals. Some of those crystals are partially replaced by goethite with microcrystals of native selenium and barite adhering to its surface (Szełęg et al. 2012). To our knowledge this is the first occurrence of native selenium in the Carpathians. In this paper we discuss the origin of the native selenium. We also provide morphological evidence of bacterial involvement in the oxidation of pyrite.

Geological setting and samples

The native selenium-bearing samples were collected in a sandstone quarry near the town of Wisła (Vistula) in the Silesian Beskid Mts (Fig. 1). The sandstone that crops out in the quarry belongs to the Senonian Lower Godula Beds of the Silesian Nappe in the western part of the Polish Outer Carpathians. The sandstone and associated conglomerate represent siliciclastic turbidites and fluxoturbidites (Cieszkowski 2004). Siliceous Godula sandstones have been classified as quartz sandstones (quartz arenites) and oligomictic sandstones (Kamieński et al. 1967). The abundance of glauconite grains in the sandstone framework is evidence of moderately reducing conditions during glauconite formation — whereas the occurrence of framboidal pyrite and pyrite-encrusted Bryozoa fossils in the sandstone framework suggest reducing conditions of the sedimentary environment or of the diagenetic environment. The fine- to medium-grained (average grain size 0.2–0.3 mm) thick-bedded sandstone in the Wisła quarry is cross-cut by numerous and rather randomly oriented calcite veins up to 4 cm thick. Vugs and drusy-cavities within calcite veins are lined by flattened rhombohedral $\{0\bar{1}2\}$ crystals of calcite up to 5 mm in size (Fig. 2A). Double-terminated rock crystals (variety known in the Carpathians as Marmaros diamond) and tabular colourless crystals of barite occur occasionally on calcite.

Numerous morphological varieties of pyrite crystals occur in calcite veins. Cubo-octahedral and octahedral crystals are the only isometric habits of pyrite observed in the veins. Predominant are distorted (axial) habits. The most common of them are pseudo-tetragonal prismatic crystals with dominant {100} faces and subordinate {210} faces, terminated by well-developed octahedral {111} faces (Fig. 2B). Other varieties of distorted crystals include pseudo-tetragonal prismatic {100} forms terminated by pseudo-pinacoid {001} and poorly-developed {111} faces, whiskers, chains of autoepitaxially aggregated cubo-octahedral crystals, and cylindrical forms terminated by {111} faces. Longer axes of distorted crystals range from a fraction of a millimeter up to a centimeter. Some of the pyrite crystals are partially replaced by goethite (Fig. 2A).

Mineral assemblages in the calcite veins represent low temperature environment as suggested by calcite crystal habit (Kostov & Kostov 1999) and the occurrence of the Marmaros diamonds. According to Karwowski & Dorda (1986) the Marmaros diamonds crystallized at 60–30 °C.

Analytical methods

Samples were examined by optical microscopy, analytical scanning electron microscopy (ASEM), electron probe microanalysis (EPMA) and X-ray powder diffraction. Crystal morphology and elemental composition of minerals were determined using an environmental scanning electron microscope Philips XL30 ESEM/EDAX (Faculty of Earth Sciences,

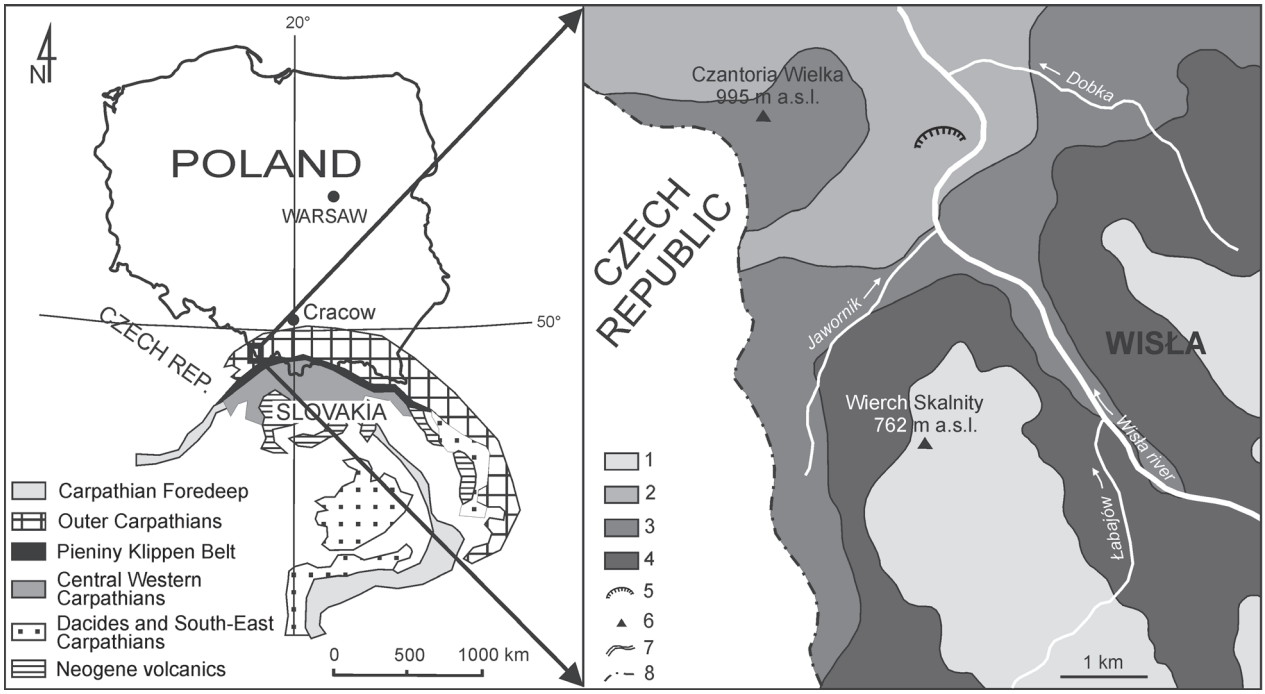

Fig. 1. Simplified geological map of the Carpathians. The enlargement shows location of the sampling site in the sandstone quarry (modified after Ryłko & Paul 1992 and Szopa et al. 2012). **1** — Upper Cretaceous-Paleogene: sandstones and shales (Istebna beds); **2** — Upper Cretaceous: sandstones and shales, Malinowskie conglomerates (upper Godulskie beds); **3** — Upper Cretaceous: sandstones and shales (midle Godulskie beds); **4** — Upper Cretaceous: sandstones, conglomerates and shales (lower Godulskie beds); **5** — sandstone quarry — sampling site; **6** — prominent mountain peaks; **7** — rivers and streams; **8** — state border.

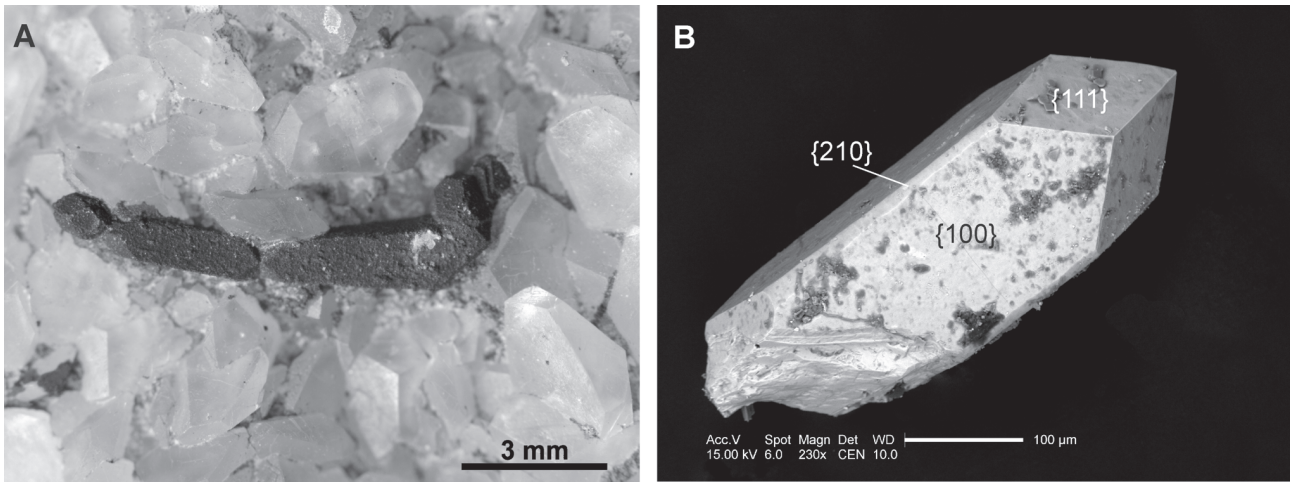

Fig. 2. A — Elongated pyrite crystal encrusted by goethite in a calcite-lined vug in the Godula sandstone. **B** — SEM image of prismatic crystal of pyrite terminated by octahedral faces.

University of Silesia). The chemical composition of the investigated minerals was determined using a CAMECA SX100 electron microprobe at the Inter-institutional Laboratory of Microanalysis of Minerals and Synthetic Materials, University of Warsaw. Electron-microprobe analyses of major elements in pyrite and goethite were performed at 15 kV and 40 nA; while the selenium in native selenium was determined at 15 kV and 20 nA. X-ray Kα lines of Fe, Cu, Mn, Zn, Ni, Co, Si, Ti and S, and Lα of Se, Te, Ba, As, Ag, Cd, Sb, and Sn were analysed using wavelength dispersive spectrometry (WDS). Minerals and synthetic materials (e.g. Bi_2Se_3 for Se) were used as standards appropriately selected for each of the analysed minerals. X-ray powder diffraction analyses of pyrite and weathered pyrite were performed using a Philips PW3710 diffractometer at the Faculty of Earth Sciences, University of Silesia under the following operating conditions: CoKα radiation, acceleration voltage 45 kV, current 30 mA, counting time 3 s per step and scan step 0.01° 2θ.

Results

Spindle-shaped acicular crystals of native selenium up to 30 μm long and 3 μm thick are adhered to the surface of goethite replacing pyrite (Fig. 3). They are often associated with platy barite in the form of barite "roses" (Fig. 3A) and occur as single crystals or sub-parallel intergrowths of split crystals (Fig. 3B–C). Native selenium has not been observed on the surface of non-altered pyrite or anywhere else in the calcite veins.

The EDS spectra of native selenium (Fig. 3D) display strong peaks of SeLα and weak peaks of iron and oxygen, most probably from the surrounding goethite. Due to the small width of the crystals it was technically impossible to obtain good quality electron microprobe data for the native selenium. The best single-spot analysis gave 80.2 wt. % Se, 0.94 wt. % Fe, 0.46 wt. % Ca, and 0.21 wt. % S. Clearly, pyrite, goethite and possibly calcite contributed to the analysis. The low analytical total (81.79 wt. %) most probably resulted from count loss. Detailed WDS scan revealed the weak peak of oxygen which can be assigned to either the surrounding material or surface oxidation of native selenium.

Goethite in the pseudomorphs after pyrite was identified by X-ray powder diffraction. Its major peaks in the X-ray pattern at 4.19 Å, 2.45 Å, 1.722 Å, and 1.698 Å are distinctly broader than peaks of pyrite. This observation suggests a low degree of crystallinity of goethite. The amount of goethite replacing pyrite in a few elongated crystals has been estimated at ca. 31 wt. % based on the Rietveld refinement. Cross-sections of the affected pyrite crystals show replacement fronts along crystal boundaries, crystal growth layers and sectors, and along randomly oriented fractures (Fig. 4). In most cases the pseudomorphic replacement of pyrite by goethite is limited to the outer portions of crystals leaving their interior volumetrically dominated by pyrite.

The surface of altered pyrite is covered by aggregates of elongated tubular structures (Fig. 5A–C). Individual tubes are tens of micrometers long and consists of granular goethite. The shape and morphology of the tubular structures closely resemble products of bacterial (e.g. *Leptothrix* sp.) iron oxidation (see, for instance figure 6 in Banfield & Zhang 2001) including goethite-encrusted filaments from oxidized pyrite ore (Hoffman & Farmer 2000). We infer

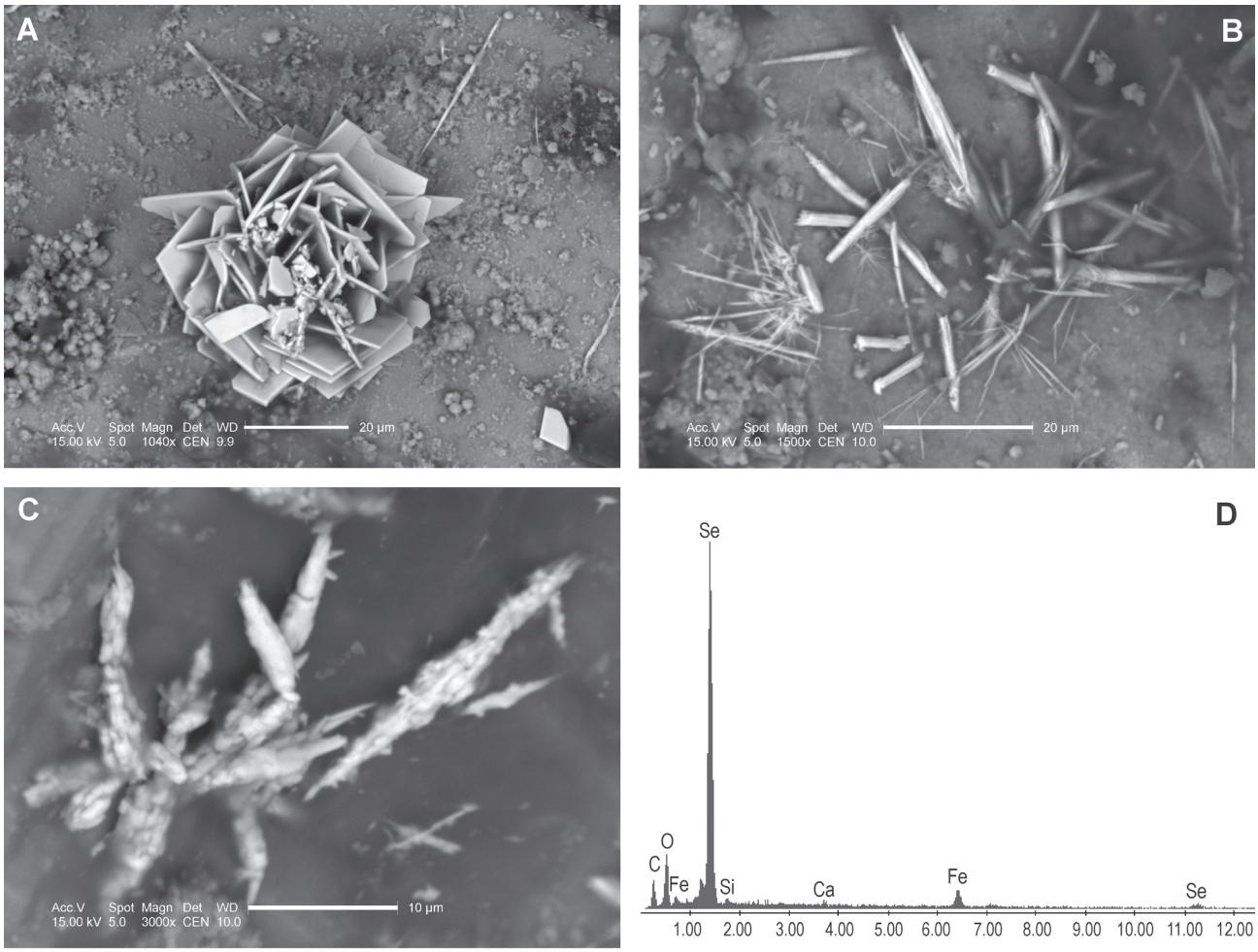

Fig. 3. A — Aggregates of platy barite crystals on the surface of goethite. Note the granular features on the surface of altered pyrite crystals and needles of native selenium. **B** — A group of native selenium crystals. **C** — Enlargement of spindle-shaped native selenium crystals. **D**— EDS spectrum of native selenium.

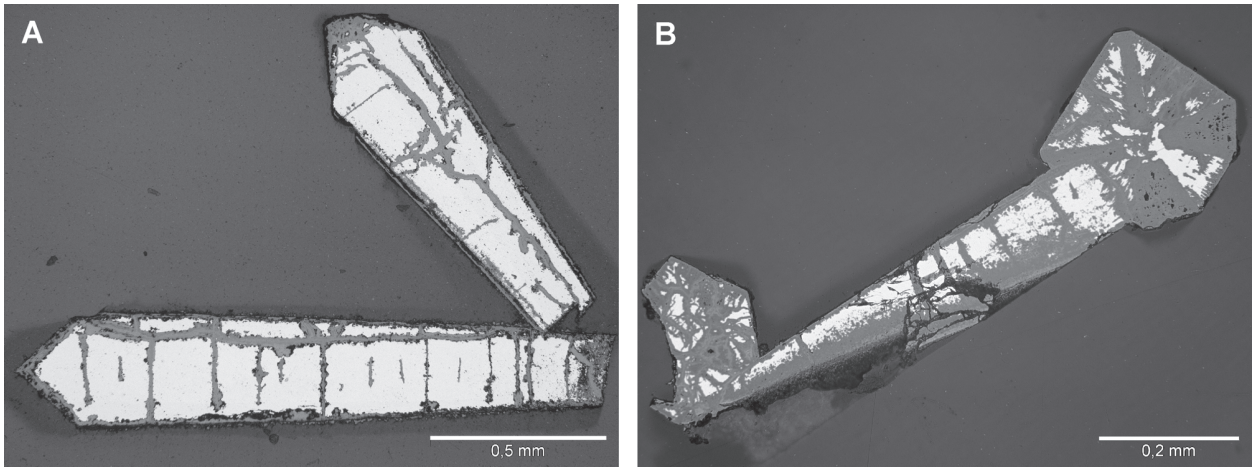

Fig. 4. Reflected light photomicrographs of pyrite crystals partially replaced by goethite. **A** — replacement of pyrite (bright) by goethite (dark) in prismatic crystals occurring along crystal faces and fractures. Fractures perpendicular to the crystal longer axis are related to growth layers in pyrite. **B** — replacement of prismatic pyrite overgrown by cubo-octahedral crystals. Note the complete removal of pyrite from the octahedral growth sectors; whereas relics of pyrite are abundant in cubic growth sectors.

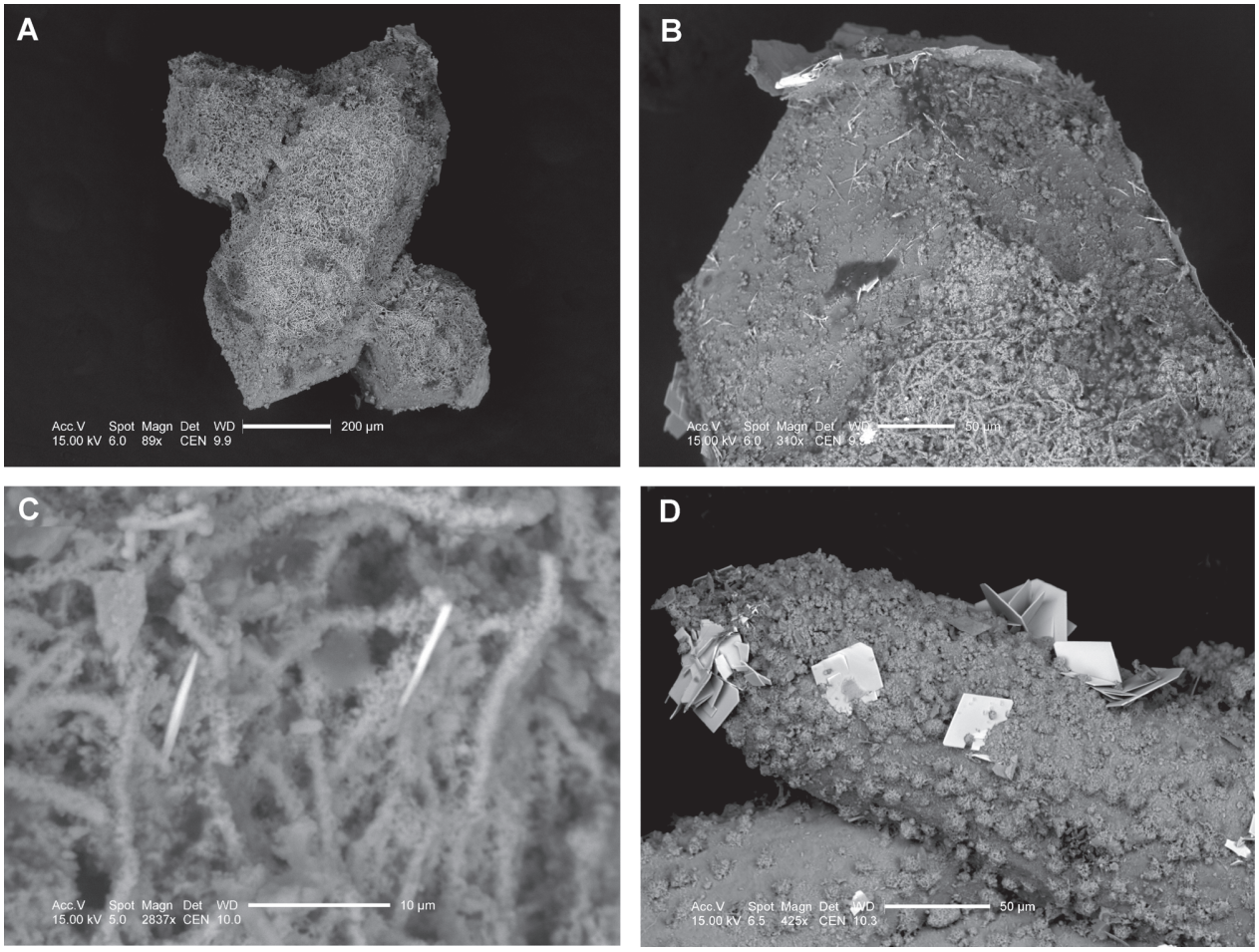

Fig. 5. SEM images of pyrite crystals covered by the goethite-encrusted filaments coalesced to forming mat-like fabrics. **A** — double-terminated prismatic crystal of altered pyrite. A mat-like texture is confined to {100} form. **B** — detail of image (A) showing the difference between {111} and {100} in the abundance of tubular sheaths of excretions of iron-oxidizing bacteria. There are only a few filaments on the octahedral faces compared to the densely covered prismatic face. Bright needles are native selenium crystals. **C** — Detail of goethite-encrusted filaments with two spindle-shaped crystals of native selenium. **D** — Granular aggregates of goethite resembling coccoids on the surface of altered pyrite. Bright platy crystals are barite.

from this striking similarity the bacterial-induced oxidation of pyrite and its subsequent partial replacement by goethite. Microbes preferentially inhabited {100} faces of prismatic pyrite crystals covering them with a dense filamentous fabric, whereas {111} were much less densely populated (Fig. 5A and B). Granular features seen on the surface of some other prismatic crystals can also be attributed to the bacterial oxidation of pyrite because of their coccoid-like morphology (Fig. 5D).

Discussion

The occurrence of native selenium in calcite veins from the Godula sandstone is confined only to the surface of goethite partial pseudomorphs after pyrite. This observation implies liberation of Se from pyrite during its microbial oxidation and subsequent precipitation of elemental selenium on the oxidized crystals. Selenium can easily be incorporated into the pyrite structure substituting sulphur due to similarities of their ionic radii (RSe^{2-} = 1.98 Å, RS^{2-} = 1.84 Å) (Coleman & Delevaux 1957; Chouinard et al. 2005). As a result, Se-bearing pyrites have been found worldwide with Se content as high as 6.68 wt. % (Zhu et al. 2004 and references therein). Average concentration of Se in pyrite is 61 ppm (Paulo & Strzelska-Smakowska 2003). Unfortunately, we were not able to determine selenium concentration in an unaltered pyrite from Wisła. However, Se concentration in that pyrite is certainly lower than its detection limit of about 200 ppm because selenium Lα X-ray line was not observed during electron microprobe (wavelength dispersion) analysis. Moreover, the small size of the native selenium crystals (Fig. 3) resulting in their small mass (on the order of fractions of a nanogram) further suggests that the investigated pyrite is not particularly rich in Se compared to other Se-bearing pyrites. Release of Se from Se-rich pyrites may lead to crystallization of millimeter- or even centimeter-sized crystals of native selenium (Zhu et al. 2004 and references therein). The unit cell parameter of the investigated pyrite (5.4174 Å) is also typical of "pure" pyrite.

Oxidation of pyrite in the calcite veins must have occurred within the pH range constrained by the calcite stability, namely in neutral or near-neutral pH conditions as suggested by the lack of dissolution features in calcite. This is further confirmed by the shape of goethite-encrusted filaments on the surface of oxidized crystals closely resembling filaments of neutrophilic *Leptothrix* sp. (Banfield & Zhu 2001). In a neutral environment abiotic oxidation of iron is efficient and rapid at high oxygen partial pressure — whereas neutrophilic bacteria are capable of oxidizing Fe(II) at low oxygen partial pressure, namely in microaerobic environments (Gault et al. 2011). That would explain why not all of the oxidized pyrite crystals are covered by mat-like aggregates of filaments. Possibly both processes, abiotic oxidation of pyrite and bacteria-induced oxidation of Fe(II) were either competing or complementary. Relatively low oxygen partial pressure may explain the partiality of pyrite oxidation.

Octahedral forms in prismatic crystals are volumetrically more profoundly replaced by goethite than prismatic forms (Fig. 4A). In cubo-octahedral crystals, the octahedral growth sectors are entirely replaced by goethite; whereas there are high amounts of pyrite relics in the cubic growth sectors (Fig. 4B). These observations are in agreement with experimental data that show higher oxidation rate of {111} growth surfaces relative to {100} growth surfaces (Guevremont et al. 1998). However, pyrite oxidizing bacteria seem to favour the opposite trend. The preferential attachment of oxidizing bacteria to the surface of {100} faces relative to {111} faces seen in samples from Wisła (Fig. 5A,B) is not accidental. Studies of surface colonization by pyrite oxidizing bacteria showed that the orientation of bacterial cells to pyrite cubic crystals was crystallographically controlled. The attached cells were preferentially aligned along [100] and [110] directions (Edwards et al. 1998). Perhaps the atomic structure of {100} faces occupied by disulphide molecules is favourable for oxidizing bacteria.

Pseudomorphic replacement of pyrite by iron hydrooxides caused release of sulphur and traces of selenium from the pyrite. Selenium Se^{2-} ions were oxidized to elemental selenium, whereas S^{2-} was oxidized to sulphate ions and bound to Ba^{2+} to precipitate barite. The source of Ba ions is not obvious, but the co-occurrence of tabular barite and calcite in the veins suggests the increased activity of barium in solution.

Oxygen partial pressure during microbial oxidation of pyrite was obviously not high enough to reach the stability field of selenates. Elemental selenium is stable in aqueous solutions over a wide range of pH and Eh values (Coleman & Delevaux 1957; Howard III 1977; Zhu et al. 2004). The stability fields of native selenium and FeOOH overlap in standard conditions in the near neutral pH range.

Acknowledgments: We thank M. Markowicz and M. Dobczyński for their assistance in sampling, T. Krzykawski for his help with X-ray powder diffraction, and M. Gardocki for sample preparation. We are particularly grateful to Igor Broska, Ruslan I. Kostov and an anonymous reviewer for their valuable comments and suggestions that substantially improved the final version of our paper. This study was financially supported by the Statutory Fund of the Chair of Geochemistry, Mineralogy and Petrography, University of Silesia.

References

Banfield J. & Zhu 2001: Nanoparticles in the environment. In: Banfield J.F. & Navrotsky A. (Eds.): *MSA Reviews in Mineralogy and Geochemistry* 44, Washington D.C.

Chouinard A., Paquette J. & Williams-Jones A.E. 2005: Crystallographic controls on trace-element incorporation in Auriferous pyrite from the Pascua epithermal high-sulfidation deposit, Chile-Argentina. *Canad. Mineralogist* 43, 3, 951–963.

Cieszkowski M. 2004: The Outer Carpathian — general geology. *Miner. Soc. Pol., Spec. Pap.* 24, 415–421.

Coleman R.G. & Delevaux M. 1957: Occurrence of selenium in sulfides from some sedimentary rocks of the western United States. *Econ. Geol.* 52, 499–527.

Edwards K.J., Schrenk M.O., Hamers R. & Banfield J.F. 1998: Microbial oxidation of pyrite: Experiments using microorganisms from anextreme acidic environment. *Amer. Mineralogist* 83, 1444–1453.

Gault A.G., Ibrahim A., Langley S., Renaud R., Takahashi Y., Boothman C., Lloyd J.R., Clark I.D., Ferris F.G. & Fortin D. 2011: Microbial and geochemical features suggest iron redox cycling within bacteriogenic iron oxide-rich sediments. *Chem. Geol.* 281, 1–2, 41–51.

Guevremont J.M., Elsetinow A.R., Strongin D.R., Bebie J. & Schoonen M.A.A. 1998: Structure sensitivity of pyrite oxidation: Comparison of the (100) and (111) planes. *Amer. Mineralogist* 83, 1353–1356.

Hofmann B.A. & Farmer J.D. 2000: Filamentous fabrics in low-temperature mineral assemblages: are they fossil biomarkers? Implications for the search for a subsurface fossil record on the early Earth and Mars. *Planet. and Space Sci.* 48, 11, 1077–1086.

Howard III J.H. 1977: Geochemistry of selenium: formation of ferroselite and selenium behavior in the vicinity of oxidizing sulfide and uranium deposits. *Geochim. Cosmochim. Acta* 41, 11, 1665–1678.

Kamieński M., Peszat C. & Rutkowski J. 1967: Petrographic variability of Carpathian sandstones and the problem of sandstone classification. *Ann. Soc. Géol. Pol.* 37, 4, 499–508.

Karwowski Ł. & Dorda J. 1986: The mineral-forming environment of "Marmaros diamonds". *Mineral. Pol.* 17, 3–16.

Kostov I. & Kostov R.I. 1999: Crystal habits of minerals. Bulgarian Academic Monographs, 1. *Prof. Marin Drinov Academic Publishing House & Pensoft Publishers*, Sofia, 1–415.

Ryłko W. & Paul Z. 1992: Geological map of Poland without Quaternary sediments. [Mapa geologiczna Polski bez utworów czwartorzędowych.] *Wydaw. kartograficzne Polskiej Agencji Ekologicznej S.A.*

Paulo A. & Strzelska-Smakowska B. 2003: Selenium at the turn of XX and XXI Centuries. *Przegl. Geol.* 51, 6, 459–464 (in Polish).

Szełęg E., Metelski P. & Janeczek J. 2012: The first occurrence of native selenium in the Carpathians. *Acta Mineral. Petrogr., Abstract Ser.*, Szeged 7, 135.

Szopa K., Gawęda A., Müller A. & Sikorska M. 2012: The petrogenesis of granitoid rocks unusually rich in apatite in the Western Tatra Mts. (S-Poland, Western Carpathians). *Mineralogy and Petrology*, Doi: 10.1007/s00710-012-0262-2

Zhu J., Zuo W., Liang X., Li S. & Zheng B. 2004: Occurrence of native selenium in Yutangba and its environmental implications. *App. Geochem.* 19, 3, 461–467.